Unsteady Non-linear Control Surface Modelling for Aeroservoelastic Applications

Lancelot, P.M.G.J.; De Breuker, R.

DOI
10.3293/asdj.2020.56

Publication date
2021

Document Version
Final published version

Published in
Journal of Aeroelasticity and Structural Dynamics

Unsteady Non-linear Control Surface Modelling for Aeroservoelastic Applications

(Received: Dec 2, 2020. Revised: Jan 15, 2021. Accepted: Jan 18, 2021)

Paul Lancelot[1]
Roeland De Breuker[1]

Abstract

In this paper, we present a data-driven method to model the unsteady non-linear response of aircraft control surfaces. This method relies on aerodynamic reduced-order models (ROM) derived from computational fluid dynamics with Reynolds averaged Navier-Stokes (CFD-RANS) analysis in the transonic domain. The ROM consists of a combination of look-up tables and transfer functions, with which we can capture the incremental unsteady loads from aileron and spoiler large deflections. The ROM can replicate transient CFD results with a 5% margin of error in most scenarios using a realistic 3D wing model. We also investigate a hybrid approach to calculate aeroelastic wing deformations. To do so, we simulate the control loads with the aforementioned ROM, while we rely on a fast but robust low-fidelity method to model the wing aeroelastic response. We compared this method against high-fidelity analysis and estimated an average error of 5% to 10% in most of the cases with a three orders of magnitude decrease in simulation time. The rapidity of such load estimation technique makes it suitable for wing sizing and flight control optimisation problems.

Nomenclature

a, b	=	Transfer function coefficients
c	=	Airfoil chord
δ_c	=	Control surface deflection (deg)
ΔCl_c	=	Incremental lift coefficient due to control surface deflection
ΔCm_c	=	Incremental roll moment coefficient due to control surface deflection
ΔQ_e	=	Incremental aeroelastic loads vector
ΔQ_c	=	Incremental aerodynamic control loads vector due to control surface deflection
ΔU_z	=	Incremental displacement due to control surface deflection
$F_{x,y,z}$	=	Aerodynamic force (N)
$G(s)$	=	Transfer function
K	=	Wing stiffness matrix
M	=	Wing mass matrix
$M_{x,y,z}$	=	Aerodynamic moment (N.m)
q_∞	=	Dynamic pressure (Pa)
s	=	Laplace variable
t	=	Time variable (sec)
$U(s)$	=	Transfer function input signal
$Y(s)$	=	Transfer function output response
ζ	=	Modal amplitude

1. Introduction

Aircraft wing control surfaces serve several purposes. Initially designed for roll control and air brake, they are sometimes used for load alleviation since the Lockheed L1011 [29]. They also may in the future be used as flutter suppression devices on large passenger jet [24]. The latter two applications are useful

[1] Faculty of Aerospace Engineering, Department of Aerospace Structures and Materials, Delft University of Technology, 2629 HS, Delft, The Netherlands

doi:10.3293/asdj.2020.56

to reduce aircraft weight and decrease their fuel consumption. Thus, the wing structural design is tied to the control surfaces performance assessment [13].
Today's aircraft sizing process still mostly relies on panel codes (doublet lattice or vortex lattice) as they are relatively accurate and very fast. However, they are limited to linear flow conditions and we cannot simulate transonic shock or flow separation with such methods. In these conditions, the load alleviation and manoeuvring capabilities of the control surfaces will also be affected. This means that a significant part of the sizing load cases for a regular passenger aircraft cannot be approximated with satisfying accuracy, leading to over-conservative load assumptions and generally heavier designs. Higher-order methods, such as computational fluid dynamics with Reynolds averaged Navier-Stokes (CFD-RANS) analyses are capable of approximating flight loads under transonic and detached flow regimes with higher-fidelity. The computational time required for such simulations is nevertheless too long to be efficiently included in the sizing process of the airframe and is usually restricted to validation purposes only.
The proposed approach in this paper aims to bring the accuracy of CFD for rapid linear aeroelastic simulations for structural sizing. This is achieved by deriving reduced-order models (ROM) of the aircraft movables from rigid CFD analyses and use these as substitutes for the loads in the aeroelastic simulation. The goal of this methodology is to remain non-intrusive and compatible with commercial analysis and optimisation tools such as NASTRAN. Building a fast aerodynamic model of the control surfaces also allows quick control optimisation to evaluate the load alleviation potential of the devices, which can in return affect the sizing of the wing box.
Fillola [10] has performed characterisation of the aircraft movables performances using CFD-RANS and compared the results to experimental wind tunnel data. This was later extended with the development of a hybrid-fidelity model developed by Bertrand [6]. Both studies were centred around the static aerodynamics of the control surfaces and showed that RANS could be used reliably for such analyses. While steady-state problems have reached a certain maturity, modelling the dynamic behaviour of control surfaces is an active topic of research. The preferred approach is usually to use reduced-order models identified from CFD [23, 21, 34, 27], as these linear models are fast enough to be used in control problems. To handle any non-linearities that may arise at transonic speeds or high deflection angles, Ghoreyshi [12] propose to perform several identifications around various deflection points.
To account for the wing flexibility, several research groups have investigated the usage of transient CFD-RANS analysis coupled with a computational structural model (CSM) in a staggered scheme [18, 5, 17, 31]. While this approach captures all the relevant non-linear aerodynamic and aeroelastic effects, it is also highly time consuming and is not suitable for aerostructural optimisation. To by-pass this issue, it is possible to perform a system identification of the aeroelastic system directly. Several papers feature this approach [16, 38, 15, 14, 33] which allows to obtain fast reduced-order models suitable for control optimisation problem. Nonetheless, full order simulations are still required for the ROM identification.
Hybrid-fidelity approaches can also be used effectively; to study the performances of a gust load alleviation system, Goggin [13] proposed to scale the unsteady aileron lift increment generated by a panel code with non-linear experimental data. More recently, Riso et al. [32] introduced a rapid simulation method to assess aileron efficiency in the transonic regime using a steady-state aerodynamic database. High-fidelity aeroelastic simulations were not required to build both models. Yet, their approaches capture some of the non-linear aeroelastic and 3D aerodynamic effects. They are however limited to quasi-steady flow corrections. A competitor of these approaches is the Hybrid Static Approach method (HSA) implemented in MSC NASTRAN [37]. It allows replacing the rigid aerodynamic component of the aeroelastic system by an external

aerodynamic database. Incremental loads from the wing aeroelastic deformation are captured using the native doublet-lattice method (DLM) solution of the software. The database, on the other hand, can be obtained from CFD or wind tunnel tests but is limited to static aeroelastic problems and linear deformations.
For unsteady problems, a similar philosophy to the HSA has been elaborated by Raveh [30], where the rigid aerodynamic contribution of a gust is computed with CFD. The unsteady aeroelastic behaviour of the aircraft is captured using a panel method. The advantage of decoupling rigid and flexible aerodynamics during aircraft sizing is evident. The flexibility of the structure can vary from one iteration to another and therefore requires a fast analysis method. The rigid part, however, remains unchanged and can be analysed using higher-fidelity tools.
In this paper, we are proposing a new way of identifying the control surface aerodynamic ROM. It only requires a single dynamic CFD simulation per flight point to identify the unsteady behaviour component of a wing movable. At the same time, the aerodynamic non-linearities are captured using look-up tables filled with steady CFD results. We have already briefly explained this approach in a previous paper[22] and we will explain it in further detail in Section 2.. Sections 3. and 5. serve as applications and validation of the method. Finally, to account for the wing aeroealstic response, we are taking a similar approach as Raveh [30]. We have also applied such scheme in [22], where we coupled our control surface ROM to the unsteady aeroelastic solution of NASTRAN. In Section 5., we will extend our analysis and compare this method against coupled high-fidelity CFD/CSM simulations.

2. Methodology behind the control surface non-linear unsteady aerodynamic ROM

Modelling dynamic aircraft response of movables using CFD is a computationally expensive process. Additionally, achieving large control rotation requires special meshing techniques not to distort the mesh excessively. A common solution to this is to use overset grids [10] [36] but such scheme requires additional modelling work and is not implemented in all CFD solvers. The method we describe in this paper proposes to separately identify the incremental non-linear steady aerodynamic contribution, ΔQ_{cs} and the linear unsteady contribution, ΔQ_{cu}. We sum these two components to obtain the full load increment value, ΔQ_c, as shown in Equation 1:

$$\Delta Q_c = \Delta Q_{cs} + \Delta Q_{cu} \tag{1}$$

We define the load increment as the variation in force and moment over the wing caused by the control surface arbitrary deflection δ_c. This is summarized in Equation 2 and is used for the steady and transient analyses.

$$\Delta Q_c = \begin{pmatrix} \Delta F_x \\ \Delta F_y \\ \Delta F_z \\ \Delta M_x \\ \Delta M_y \\ \Delta M_z \end{pmatrix} = \begin{pmatrix} F_x - F_x(\delta_c = 0) \\ F_y - F_y(\delta_c = 0) \\ F_z - F_z(\delta_c = 0) \\ M_x - F_x(\delta_c = 0) \\ M_y - F_y(\delta_c = 0) \\ M_z - F_z(\delta_c = 0) \end{pmatrix} \tag{2}$$

When looking at control surfaces, a non-linear steady aerodynamic behaviour can be characterised by a non-linear relation between the deflection angle and the resulting incremental lift and moment. This can be identified using steady-state CFD simulations for a range of movable settings. The resulting loads can be stored in look-up tables, as shown in Figure 1. Such simulations are much faster to compute than transient solutions and do not require dynamic mesh

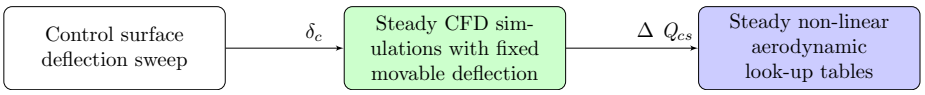

Figure 1: Steady aerodynamic modelling to capture large control surface deflection responses.

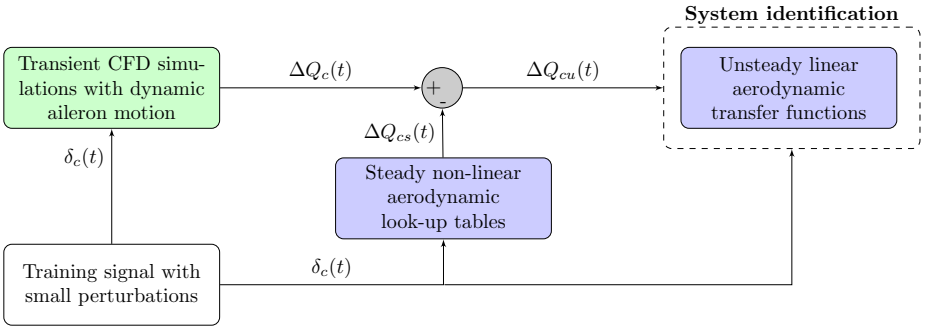

Figure 2: Transfer functions identification procedure.

deformation. Therefore, this approach can be easily scaled to include multiple flight points and configurations. This method is not restricted to CFD-RANS, and wind tunnel results or high-order method, such as Zonal Detached Eddy Simulation (ZDES), could be used instead[11].

Unsteady effects around control surfaces, such as the aerodynamic response phase lag and amplitude changes due to the frequency of actuation, can be captured using transfer functions derived from unsteady CFD analysis. To avoid any excessive grid distortion, we are performing the analysis with small deflection amplitudes. These make it easier to handle mesh deformation for the CFD solver with a smoothing deformation technique [1].
The transfer functions $G(s)$ gives the relation between an input U(s) and output Y(s) in the Laplace domain:

$$G(s) = \frac{Y(s)}{U(s)} = \frac{b_m s^m + b_m - 1 s^m - 1 + ... + b_1 s + b_0}{a_m s^m + a_m - 1 s^m - 1 + ... + a_1 s + a_0} \tag{3}$$

$G(s)$ matches the phase shift and amplitude of the response to the input. In our case, $U(s)$ and $Y(s)$ are the Laplace transforms of the $\delta_c(t)$ and $\Delta Q_{cu}(t)$. $\delta_c(t)$ is an arbitrary deflection command for the control surface given in the time domain. $\Delta Q_{cu}(t)$ is the incremental unsteady load response due to a dynamic surface deflection. We obtain $\Delta Q_{cu}(t)$ by removing the quasi-steady non-linear component $\Delta Q_{cs}(t)$ from the control load increment $\Delta Q_c(t)$. This operation is shown in Figure 2 and is required because the transfer function we use is only valid for approximating linear time-invariant system. We achieve the identification of the transfer function polynomials using Matlab TFEST toolbox [4]. Their orders can vary from 2 to 4. The objective is to minimise the transfer functions complexity while maintaining a fitting value above 90%. In the 3D example Section 4., this threshold value was lowered to avoid over-fitting in areas where we had issues getting a good fit from the Matlab TFEST function, but did not compromise the overall quality of the ROM.

Following the process shown in Figure 3, we combine the results produced by the look-up tables and the transfer functions to capture the full response. We run our ROM using the Simulink platform [3] which handles both time and frequency domains. In Section 3., we assess the accuracy of this method on a 2D example.

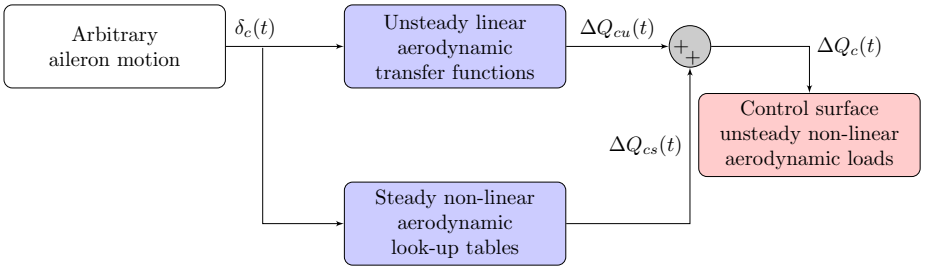

Figure 3: The unsteady non-linear aerodynamic ROM is comprised of the look-up tables and the transfer functions.

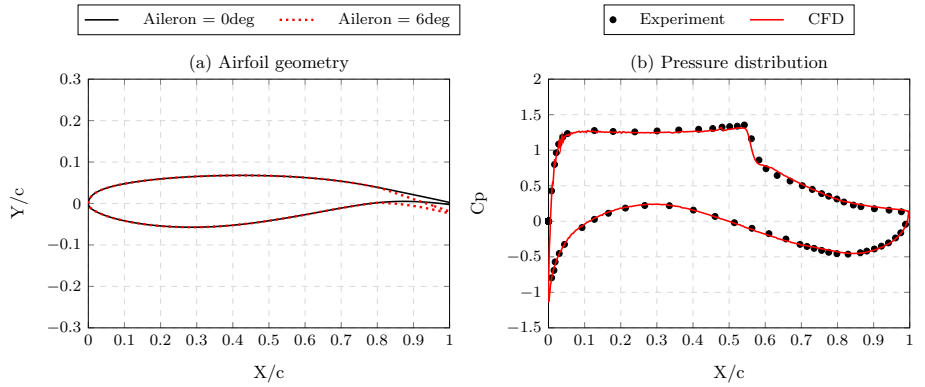

Figure 4: In (a) is the OAT15A airfoil geometry and in (b) the pressure distribution with the aileron deflected at 6 degrees.

3. Application to a 2D case with the OAT15A airfoil

3.1 Validation of the steady CFD setup

To assess the validity of the modelling approach presented in Section 2., we are doing the identification using the Onera OAT15A airfoil equipped with an aileron. The airfoil geometry is shown in figure 4. We perform CFD using Ansys Fluent with a RANS K-ω SST turbulence model [2]. Steady wind tunnel results for this airfoil are used as validation, in the conditions described by Fillola [10]. The airfoil angle of attack is set at 1.5 degrees, the aileron is deflected down by 6 degrees, and the Mach number is M=0.73. The transonic shock is visible on the pressure coefficient plot, and we can see a good agreement between the CFD results and the experiment.

3.2 Identifying the aileron ROM

For the subsequent study, we look at a 20 times scaled-up version of the original OAT15A. We scaled it up to have the aileron actuation speeds and reduced frequencies closer to a full-scale aircraft wing. This way, it is easier to assess if our method is valid for typical ailerons band-with. The airfoil is set to 0 degrees angle of attack (AoA), as we are mostly interested in load increments from control deflections. Incidence effects between the wing AoA and the lift increment are not considered. The static aileron sweep in Figure 5 highlights the non-linearity of the lift increment. This can be explained by the shock position moving downstream when the aileron is deflected down, as shown in Figure 6. The linear region in Figure 5 is sustained longer for high negative deflection angles due to the shock being mitigated on the upper surface of the wing when the aileron is deflected up. Similar observations were already made by Fillola [10].

We describe the four steps to create the aerodynamic ROM as follow:

i) We first perform a dynamic CFD simulation, where the aileron deflection is driven by a square command $\delta_c(t)$ varying from -2.5deg to +2.5deg as shown in In Figure 7 (a). The resulting incremental lift $\Delta Cl_c(t)$ from the aileron motion is plotted in Figure 7 (d).

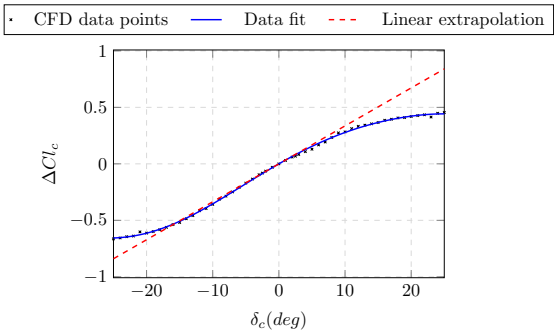

Figure 5: Lift coefficient increment from -25 to +25 degrees aileron deflections. The fitted data is used for the look-up table in the aerodynamic ROM. The linear extrapolation is performed around the neutral aileron deflection.

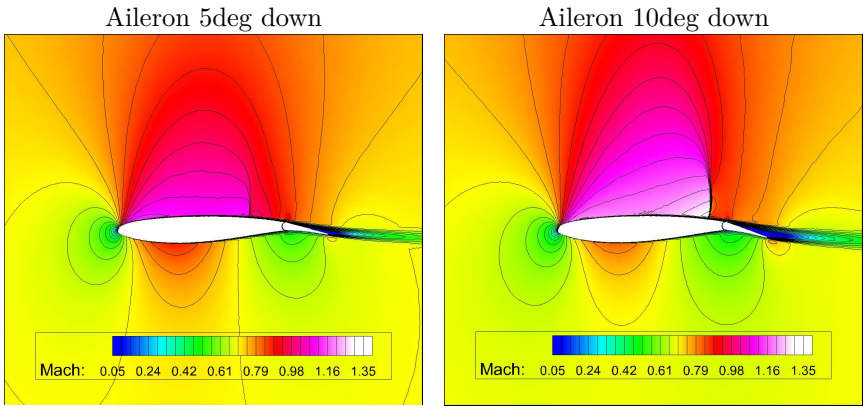

Figure 6: Mach flow contours around the airfoil with AoA = 0deg. The shock moves downstream as the aileron is deflected down.

ii) We create a non-linear quasi-steady lift response $\Delta Cl_{cs}(t)$ from the aileron command using the look-up tables, plotted in Figure 7 (b). The process to create the look-up tables is straightforward, as shown in Figure 1 and only requires steady-state CFD analysis. In this example, the aerodynamic database is comprised of 53 simulations results going from -25deg to +25deg aileron deflection angles. A convergence study was not performed to determine the adequate number of steady simulations to run. However, we observed on the 2D example that the use of a polynomial fitting function (as shown in Figure 5) to smooth the static response was giving better results on the hysteresis plots (Figure 8 and 9) than an interpolation between the points stored in the look-up tables.

iii) The non-linear quasi-steady lift response $\Delta Cl_{cs}(t)$ is subtracted from the transient CFD response $\Delta Cl_c(t)$, to extract the unsteady lift component $\Delta Cl_{cu}(t)$ from the aileron motion. We explain this operation in Figure 2. By doing this, we make sure to perform the transfer function identification over a linear signal. In Figure 7 (c), we see a very good match, within 1% error, between the transfer function and the training data obtained from CFD.

iv) We recompose the full response $\Delta Cl_c(t)$ by summing the non-linear quasi-steady lift increment $\Delta Cl_{cs}(t)$ with the linear unsteady lift increment $\Delta Cl_{cu}(t)$, as we depicted in Figure 3. We can see from the comparison with the CFD in Figure 7 (d) a good accuracy of our model, within 1%. While the amplitude of the deflection signal is moderate, we can already notice some non-linearity on how the lift increment is not exactly proportional to the deflection angle. Along with the unsteadiness, this effect is well captured using the steady look-up tables.

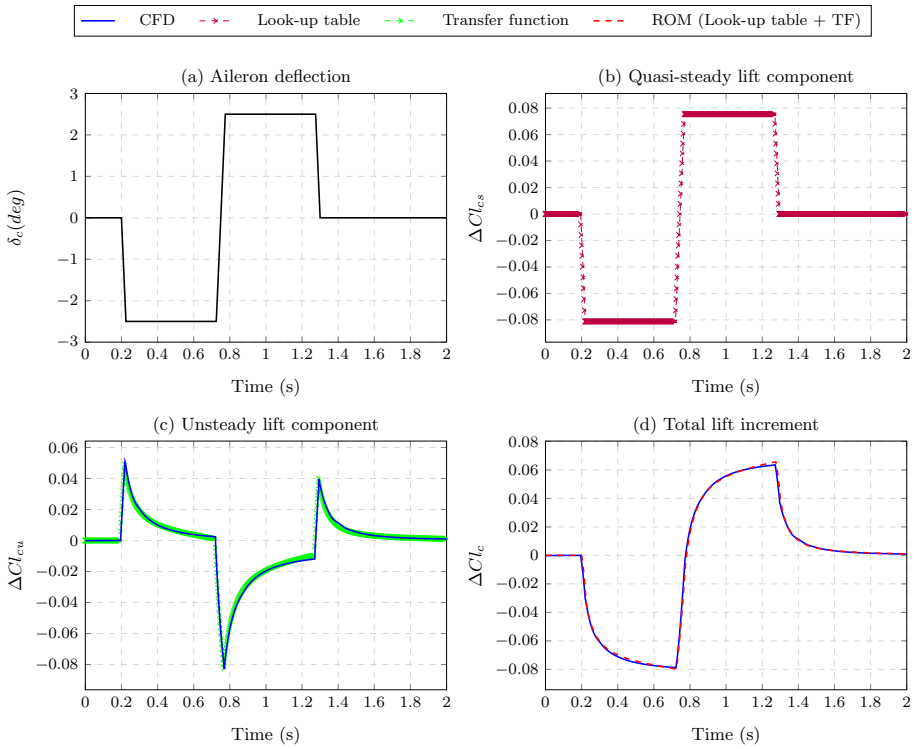

Figure 7: Unsteady non-linear lift increment modelling components.

3.3 Comparison against unsteady CFD for a range of amplitudes and frequencies of aileron oscillation

The model described above is tested on signals varying from ±1 to ±15 degrees of deflection, and from 0,5Hz to 8Hz in frequency. Such amplitude range is typical for the GLA function using the ailerons [35, 6, 28], for which they have to rotate rapidly. We show the results against the CFD responses in Figure 8. Overall, the model gives good prediction for aileron deflection rates up to 60deg/sec. This rate is considered to be practical for active load alleviation, as shown by Pusch et al. [28]. Furthermore, motions with high deflection amplitudes but moderate frequencies are also well captured.

In figure 9, we select a few cases where we also show the comparison against the non-linear quasi-static model and a linearised unsteady model. The latter is obtained by substituting the non-linear steady look-up table used in the ROM by a linear approximation such as the one we show in Figure 5. The unsteady component of both non-linear and linear models remains identical.

We see that the quasi-steady model gives results which are too optimistic in term of lift increment and do not account for the phase shift, as shown by the lack of hysteresis in the response. The linearised model gives closer results to our ROM for small deflections but loses in accuracy for higher deflection amplitude by also being too optimistic.

4. Control surfaces ROM applied to a 3D rigid wing

4.1 uCRM model with aileron and spoiler

The methodology we described in Section 2. is applied to a 3D wing. This wing is the undeformed common reference model (uCRM) developed from the NASA CRM by Brooks et al. [7]. We have modified it to include an aileron and a spoiler as depicted in Figure 10.

For the 3D rigid wing study, we use Ansys Fluent with a $k-\omega$ SST two equations turbulence model [2]. The flow Mach number is set to M=0.85 with a dynamic pressure of 11.100 Pa, representative of a typical airliner at cruise.

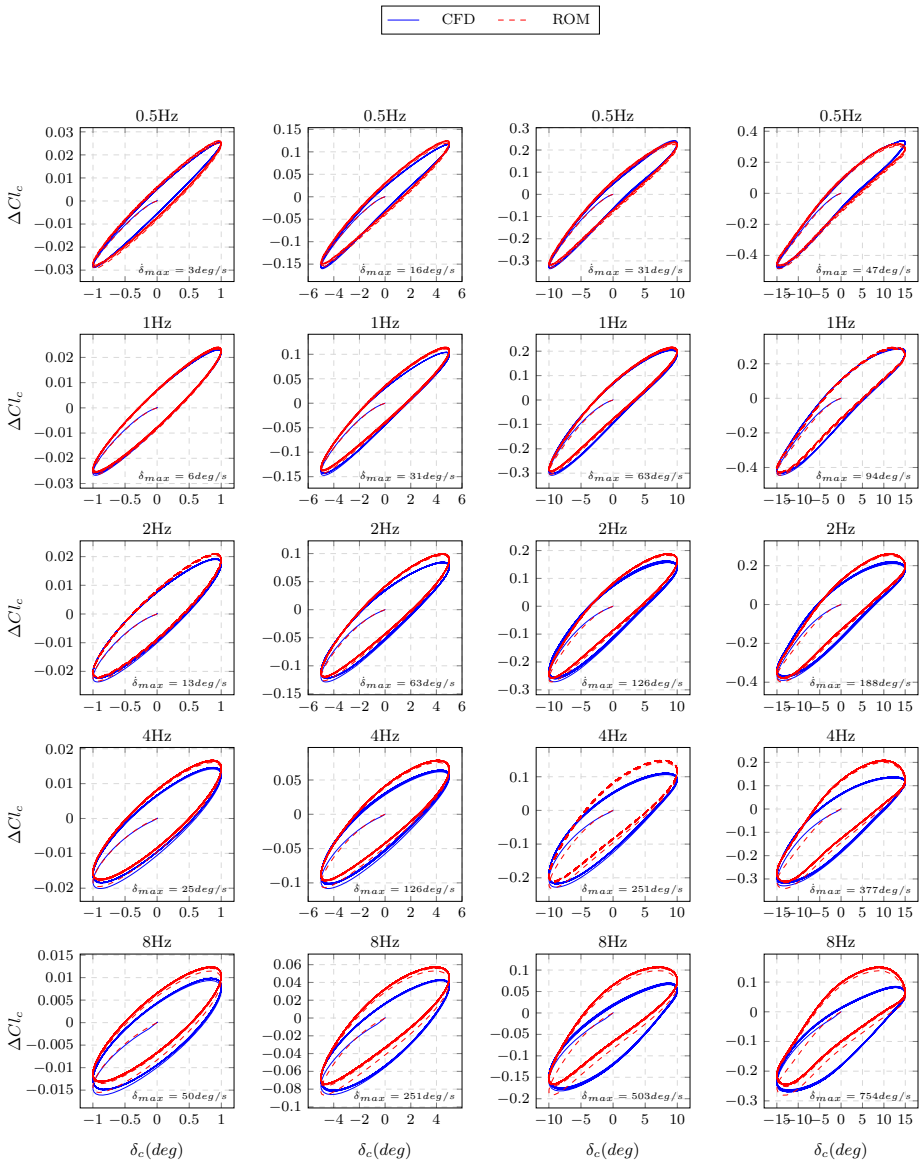

Figure 8: Dynamic aileron lift increment plotted against the deflection angle for different amplitudes and frequencies of actuation.

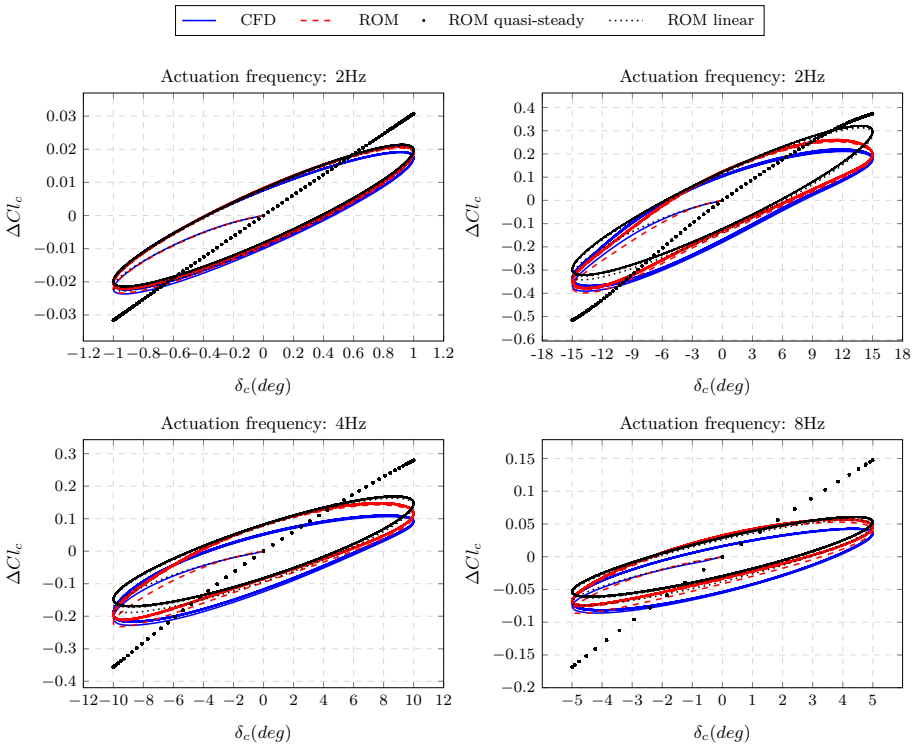

Figure 9: Dynamic aileron lift increment plotted against the deflection angle for a selected set of amplitudes and frequencies of actuation.

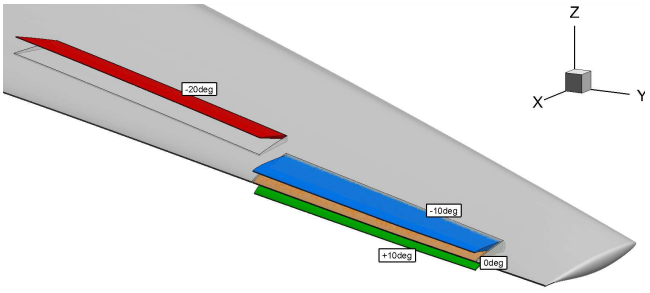

Figure 10: uCRM wing model fitted with a spoiler and an aileron.

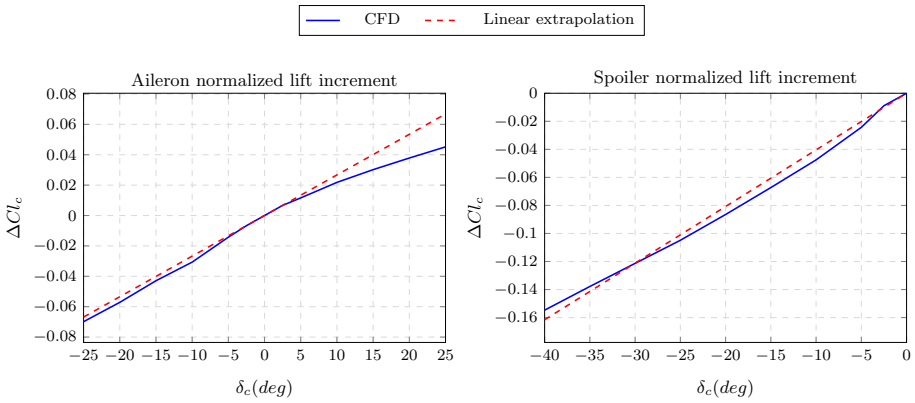

Figure 11: Lift increment obtained on the 3D wing for the aileron and the spoiler. The linear trends are extrapolated around the 0 degree position for the aileron, and with a least square fit for the spoiler.

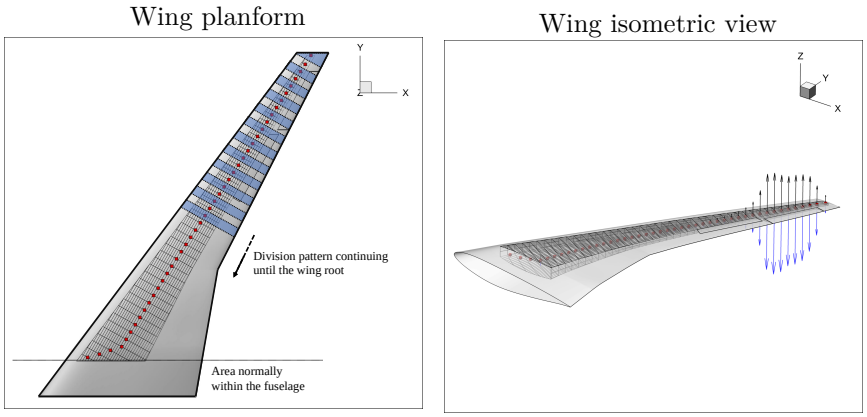

Figure 12: The wing outer mould and control surfaces are overlaid with the wingbox structural model. The red squares represent the condensed DOF on which the CFD aerodynamic loads ΔQ_c from each strip are integrated.

Simulations are achieved with an aircraft AoA of 0 degrees. As for the 2D example in Section 3. , non-linear aerodynamic effects arise when deflecting the control surfaces. In Figure 11, the lift increment from the aileron deflection largely deviates from the linear trend, when deflected down. Similarly, the spoiler, when deflected up, exhibits a non-linear behaviour, especially at low deflection angles less than 15 degrees.

For the 3D simulations, we need to capture in the spanwise direction the changes in lift and moment due to the control surface deflection. These changes vary well beyond the control surface location as shown in figure 14. Therefore, the wing is divided into strips on which the aerodynamic loads are collected. Each strip corresponds to the location of one of the condensed structural degrees of freedom (DOF). These strips are defined as shown in Figure 12.

4.2 Comparison against unsteady CFD for different control signals

We identify the loads on each strip following the same process as described in Section 2.. To build the look-up tables for the 3D wing, we perform the CFD analyses with control deflection increments of 5 degrees, with additional points at -2.5 and +2.5 degrees. Unlike the 2D example, the reduced number of steady simulations stored in the look-up tables means that interpolating between the points is preferable over a polynomial regression, to avoid over-fitting. For the unsteady identification, the training signal used for the aileron is a square command moving from -5.7 to +5.7 degrees deflection, as shown in Figure 15. A similar signal is used for the spoiler, but centered around a baseline deflection of 20 degrees. For the dynamic simulations, we set the time step to 0.01 seconds.

We show the results of the identified models for the aileron and the spoiler in Figure 13:

If we take two slices for each graph at 1 and 2 seconds, as shown in Figure 14, we see that the maximum error in the incremental lift in the spanwise direction is small, in the order of 5%. We see that the effects of the aileron and spoiler

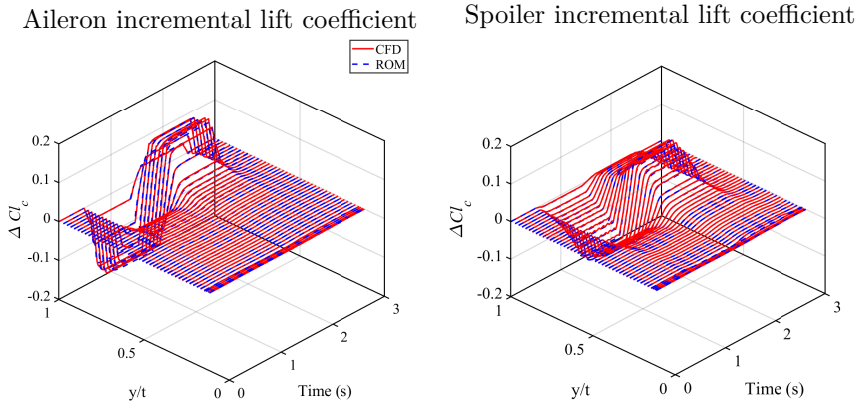

Figure 13: Time dependent visualization of the spanwise lift increment during the aileron and the spoiler dynamic deflections.

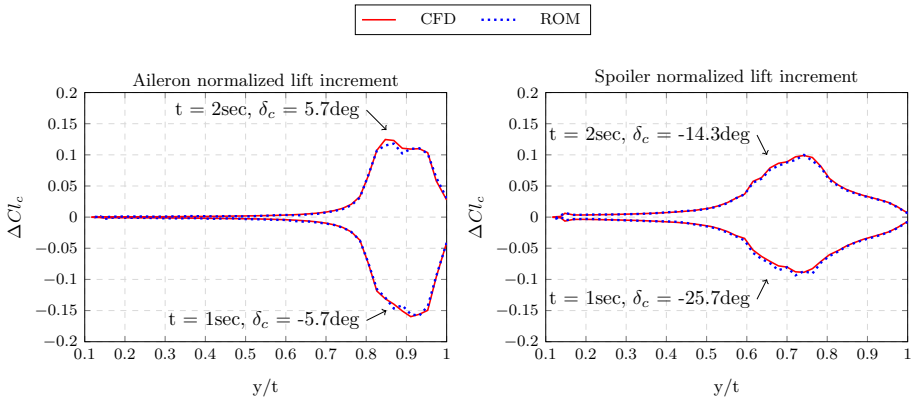

Figure 14: Rigid aileron and spoiler lift increment over the span. The spoiler lift increment is zeroed around a 20 degree baseline deflection angle.

deflections extend on a significant portion of the wing. This is well captured by our model since we perform the identification on the entire 3D wing.

When looking at the integrated incremental loads (ΔCl_c and ΔCm_c) in Figure 15 we also see that the ROM produces good results compared to the rigid CFD analysis, usually well below a 5% error. For the "square" signal, the aileron deflects up and down at a velocity of 57.3deg/sec, while for the "triangular" signal, the deflection speed varies from 14.3 to 114.6deg/sec. A deflection rate close to 60deg/sec is practical for active load alleviation, as outlined in Section 3.3. We can conclude from these results that the ROM is effective for a wide range of deflection speeds. Additionally, despite a reduced number of points stored in the look-up tables compared to the 2D example, the ROM still maintains a good accuracy.

The spoiler results are particularly relevant because there is no widespread aerodynamic model for this type of control surface aside from high-fidelity CFD or empirical formulas [8]. Due to limitations in our CFD setup, we are here looking at a piecewise comparison between the ROM and the rigid CFD. We are indeed limited to the amplitude at which we can deflect the spoiler without distorting excessively the mesh. The ROM for the spoiler is generated following the same process as for the aileron. We only need to perform the unsteady identification around a single spoiler deflection, here at 20 degrees. Leaning on this single model, the results in Figure 16 show good agreement for the whole range of deflections within 5%.

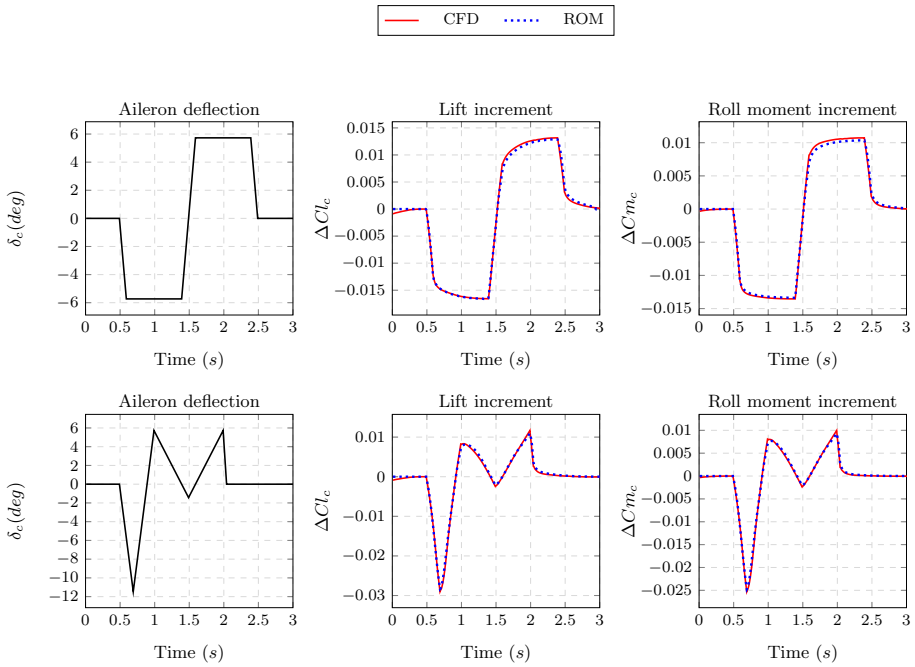

Figure 15: Time dependent visualization of the lift and bending moment increment coefficients for various aileron dynamic deflections.

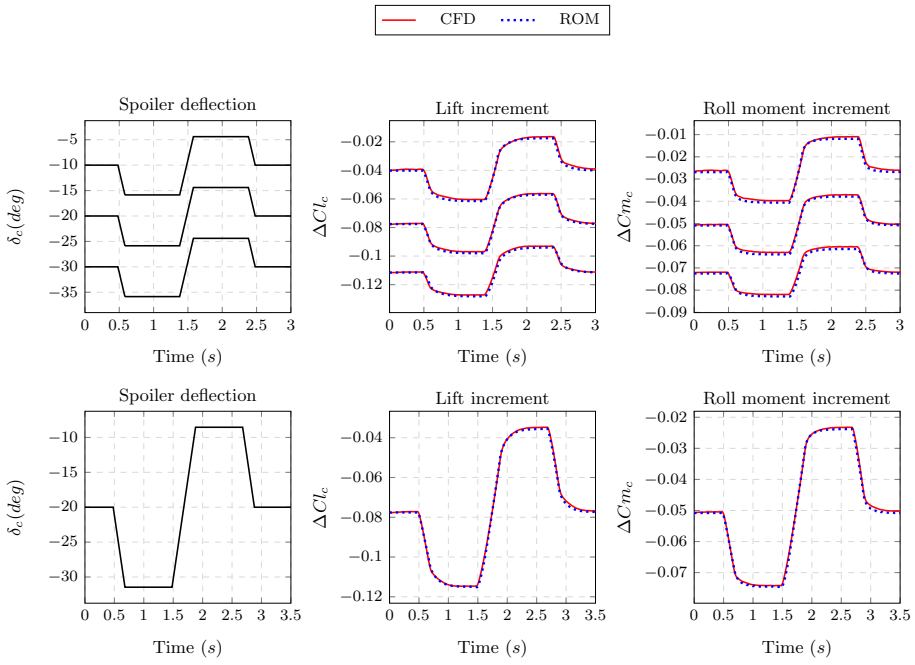

Figure 16: Time dependent visualization of the lift and bending moment increment coefficients for various spoiler dynamic deflections.

5. Control surfaces ROM applied to a 3D flexible CRM wing

5.1 Hybrid aeroelastic methodology

Transport aircraft wings are not rigid, and their flexibility has a significant impact on control authority. During their sizing, several iterations are needed to converge to the optimal structural and control design variables. This requires many aeroelastic analysis and thus prohibits the use of a purely high-fidelity method. Additionally, free-flying flexible analysis to simulate complex manoeuvres or gust encounter are very costly to perform using coupled CFD/CSM.
To resolve this situation, we choose to combine our aerodynamic control surfaces ROM to a low fidelity unsteady aeroelastic solver relying on the linear Doublet Lattice Method (DLM) panel method [19]. In cruise flight, we assume that the main source of aerodynamic non-linearity mostly comes from the control surface deflection, and not from the wing elastic response itself, which would remain mostly linear. In our model, transonic incremental loads on the wings ΔQ_c, are only a function of the deflection command δ_c, as shown in the aeroelastic equation of motion shown in Equation 4 on the right-hand side. M and K are the aircraft mass and stiffness matrices derived from MSC NASTRAN. ΔQ_e is the generalized aerodynamic forces from the wing elastic response and is obtained from the DLM method, embedded in MSC NASTRAN. M_c is the control surface mass matrix but is neglected in our analysis and q_∞ is the dynamic pressure. ζ is the modal displacements vector while s is the Laplace domain variable. This approach can also be used to include high-fidelity rigid gust loads as shown by Raveh [30].

$$([M]s^2 + [K] + q_\infty[\Delta Q_e(s)])\zeta(s) = -([M_c]s^2 + q_\infty[\Delta Q_c(s)])\delta_c(s) \qquad (4)$$

We describe the integration of the model in Figure 17. The MSC NASTRAN dynamic aeroelastic module (SOL146) is used to solve the system in the frequency domain [19]. However, the aerodynamic loads due to the aileron deflection ΔQ_c are included through time domain direct force inputs (DLOAD tables [25]). MSC NASTRAN converts them to the frequency domain using the Fourier transform. For every condensed structural DOF on the flexible wing, we derive one matching aerodynamic local ROM ΔQ_{ci}. This allows capturing the load increments along the wingspan from the movable deflection δ_c. We build the ROMs for the incremental forces in the z and moments in the y directions only, which is deemed to provide enough accuracy as the comparison in the next section shows. In this exercise, however, the control surfaces structural properties and interfaces with the wing are not included.

With this setup, we can then extract the loads and stresses on the entire aircraft in the time domain from MSC NASTRAN. Our method retains some of the important non-linearities, while greatly simplifying the rest of the simulation. In a structural sizing exercise, we could therefore quickly update our structural wing design because SOL146 is relatively cheap to run while keeping the ROM untouched. Also, because the method is relatively non-intrusive, we could rely on a different aeroelastic model, such as unsteady vortex lattice (UVLM) or linearised CFD for improved fidelity.
In the next section, we will test our assumption against traditional high-fidelity FSI analysis. We will focus on the incremental flexible loads caused by control deflection δ_c only, as several correction methods already exist for improved steady aeroelastic analysis [37, 9].

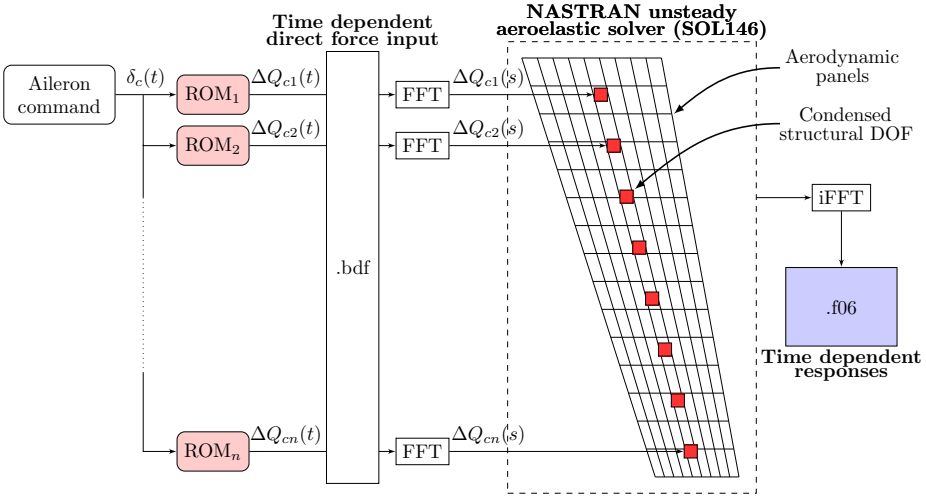

Figure 17: Hybrid unsteady approach: we add the control loads generated by the aerodynamic ROMs to the MSC NASTRAN aeroelastic solver.

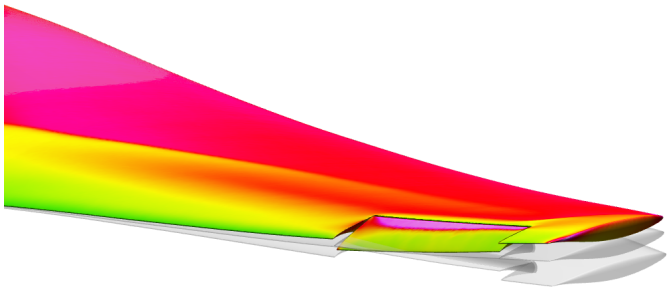

Figure 18: Illustration of a dynamic aileron deflection using high-fidelity CFD/CSM simulation.

5.2 Comparison against high-fidelity FSI

We perform a comparison of our hybrid approach against a traditional high-fidelity FSI using a time domain staggered scheme. It is adapted from the coupled CFD/CSM framework developed by Piñeiro Rielo [26] to handle control surface motion as illustrated in Figure 18. A Newmark scheme is used to solve structural dynamics. The stiffness and mass matrices are extracted from MSC NASTRAN using the DMIGPCH command [25]. The CFD simulation is run with Ansys FLUENT using a k-ω SST turbulence model and time steps of 0.01sec. Mesh deformation is achieved with a smoothing deformation technique [1] and therefore limits the maximum deflection achievable. The wing displacements are extrapolated from the structure deformation via radial basis functions (RBF) implemented with a user-defined function (UDF) in Ansys FLUENT. The CFD loads are transferred back to the structure using the nearest neighbour approach.
For this comparison, it is important to have consistent settings between the simulations needed to identify the ROM and the high-fidelity reference simulations. We looked at two different wing stiffness behaviours as shown in Table 1. This range is conform to modern airliners in service today [35]. Regarding our hybrid model, we use the 50 first modes during the NASTRAN analysis. While wing A and B have the same mass configuration, wing B has a wing material stiffness twice lower than wing A, which allows a higher wing deformation.

In Figure 19, we show a time comparison between our hybrid approach and the high-fidelity FSI analysis. The ROM is identified in Section 4., from a single rigid transient CFD analysis and in this case, 15 rigid static analyses with a range of control surfaces deflections going from -25 to +25 degrees. We identify one ROM per type of control surfaces and per Mach number. A single ROM supports any arbitrary control motion, and the loads ΔQ_c can be scaled

mode	wing A	wing B
1st	2.96	2.09
2nd	7.53	5.32
3rd	8.34	5.90
4th	13.08	9.25

Table 1: Frequencies in Hz of the two models.

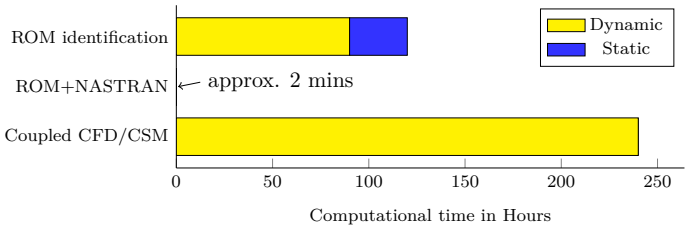

Figure 19: All CFD simulations run on a 32 cores Intel CPU clocked at 2.30Ghz. Simulink and NASTRAN analyses run on a single core.

up with the dynamic pressure q_∞. The accuracy of such scaling is however beyond the scope of this paper, and all the subsequent simulations are run at a fixed Mach 0.85 and $q_\infty = 11.100$Pa. When it is combined with MSC NASTRAN SOL146, the wing mass and stiffness properties can be varied at minimum cost. Therefore, this solution is a lot less time consuming than direct a coupled CFD/CSM high-fidelity analysis. Also, because static aerodynamic CFD analyses are comparatively cheap to perform (about 2 hours per deflection setting and flight point), the aerodynamic look-up tables can be refined at a relatively low computational cost.

5.3 Flexible wing and aileron results

As for previous results in this paper, we only look at the load and displacement increments induced by the aileron and spoiler deflections. The wing AoA is set to 0 degrees. In Figure 20, we deflect the aileron from -5.7 to +5.7 degrees. We are comparing three different wings: one rigid, and two flexible wings: A and B.
Due to an excessive mesh deformation, the simulation with the B model crashed before the end. This shows the difficulty of modelling such problem using a high-fidelity method, but the authors still deemed these results relevant for comparison. Looking at the wing tip vertical displacement ΔU_{ztip}, we see that the amplitudes are in the same order of magnitude for both the FSI and the hybrid model. The relative error is however higher for wing B and reaches 13% during the negative displacement peak. The error in the stiffer wing A remains below 12%. When looking at the incremental lift coefficient ΔCl_c and roll moment ΔCm_c, we see similar trends for the tip displacement where the stiffer wing and the rigid wing have a lower error at the peak values, around 5%, as compared to the more flexible wing. We also see that the amplitudes are different when deflecting the aileron up or down, highlighting aerodynamic non-linearities which our ROM captures effectively. Finally, we see that the rolling moment and lift coefficients significantly reduce when the wing stiffness is decreased. This aeroelastic effect is fully captured by our hybrid model. It can lead to control reversal and is a key driver of the aircraft sizing, as the wings may have to be reinforced to avoid such issue[20].

In Figure 21, we test our hybrid approach with a different deflection signal, moving the aileron from -11.4 to +5.7 degrees. The deflection speed varies from 14.3 to 114.6deg/sec while the flight parameters remain the same as the previous set of simulations. This command signal is arbitrary but covers a realistic range of deflection rates. We see a good agreement overall for both the rigid and the flexible wings.

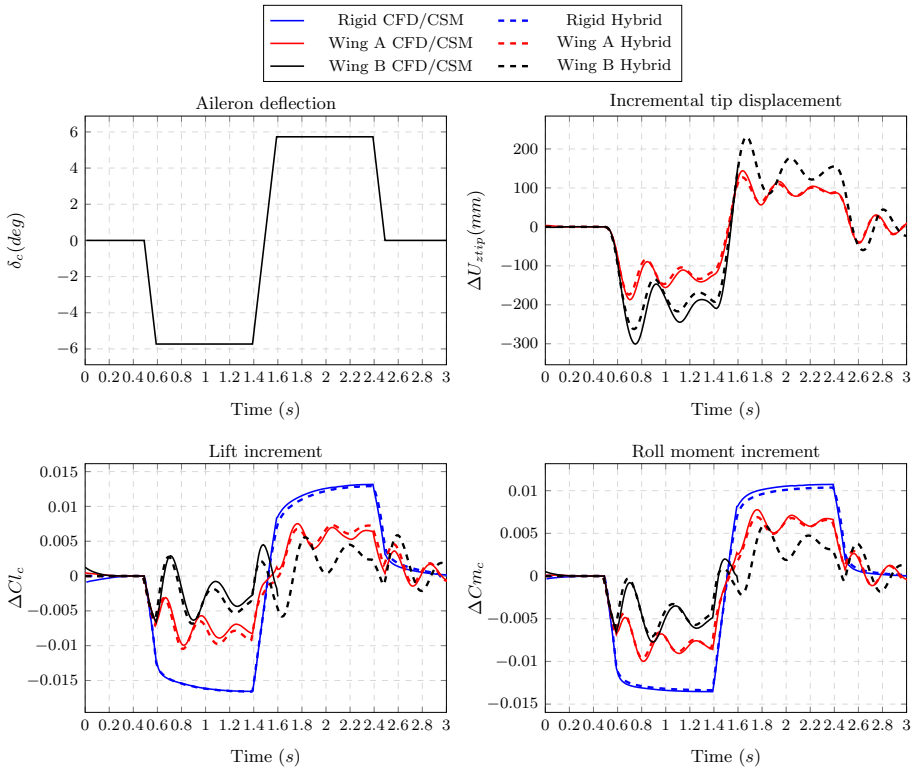

Figure 20: CFD/CSM compared against the hybrid model with dynamic aileron deflections. The deflection range varies from -5.7 to +5.7 degrees.

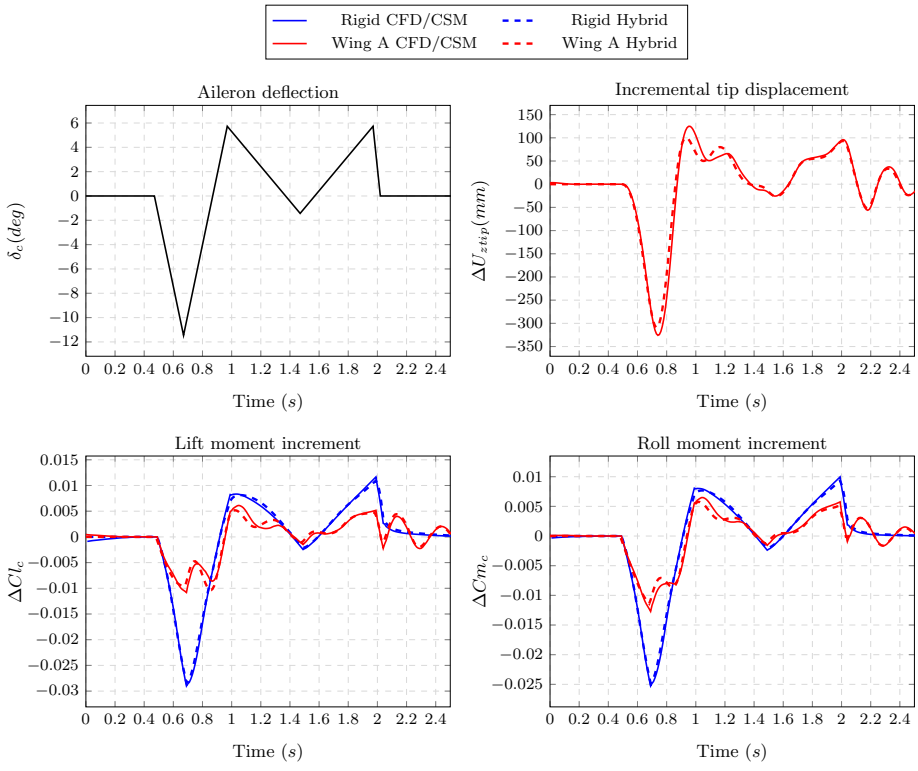

Figure 21: CFD/CSM compared against the hybrid model with dynamic aileron deflections. The deflection range varies from -11.4 to +5.7 degrees.

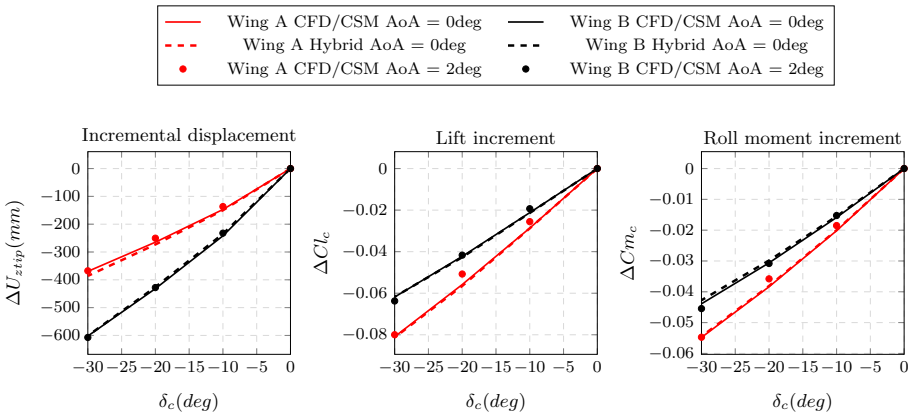

Figure 22: CFD/CSM compared against the hybrid model with static spoiler deflections.

5.4 Flexible wing and spoiler results

When comparing the results for the spoiler deflection, we are limited by the range of dynamic deflection possible with our CFD and mesh deformation setup. To avoid distorting the mesh excessively around the spoiler, we perform a piecewise comparison of our hybrid model against several FSI runs with the spoiler positioned at 10, 20 and 30 degrees. As for the aileron, the spoiler ROM identification only needs a single small disturbance transient CFD analysis to capture the unsteady flow response to the movable deflection, and a set of 9 steady CFD simulation from 0 to -40 degrees to capture the non-linear aerodynamic response at large deflections.

We start the comparison with steady aeroelastic results plotted in Figure 22. Results at the 0 degrees AoA generally match well, with errors ranging from 0.17% to 5% for both wing type in vertical tip displacement, lift and moment coefficients.

We also looked at the possible interactions between the spoiler deflection and the aircraft AoA. In their combined wind tunnel and numerical studies, Wiart et al. [39] showed that limited coupling could be observed at small AoA (less than 2 degrees) in the aileron response. However, for the spoiler, Wilkilson [40] described the risk of spoiler rigid aerodynamic reversal at transonic speeds and positive aircraft angles of attack. They explained it by the complex shock motion being influenced by both the aircraft incidence and the spoiler setting. In our results, we can also see higher discrepancies at 2 degrees AoA between the CFD/CSM analyses and our hybrid approach. Nonetheless, it remains comparatively small. Despite the aircraft incidence increasing, the wing washout limits the local angle of attack, and hence the shock motion due to the change in AoA. Further evidence of this is in the lesser error with the more flexible wing B. While wing A results have an error as high as 12.7%, the wing B has a maximum response error of only 6% compared to the hybrid approach, which relies on a ROM identified at an AoA of 0 degrees.

For the unsteady cases, we show in Figure 23 the results for a dynamic spoiler moving from -5.7 to +5.7 degrees around a baseline deflection of 30 degrees with the aircraft AoA at 0 degrees. We compared the rigid wing, and the wings A and B, in a similar setup as for the aileron. The results have been zeroed around this baseline spoiler position. For ΔU_{ztip}, ΔCl_c and ΔCm_c, we have a good agreement between our hybrid model and the CFD/CSM simulations. The error at the peak values is at a maximum of 5.2%. The results for the spoiler are generally better than for the aileron. We attribute this to the lower wing deformation induced by the spoiler deflection. It is due to its more inboard position and therefore its lower influence on the wing bending. Similarly, we observe a lower decrease in spoiler effectiveness as the stiffness is reduced. We can also conclude that our hybrid approach could perform equally well in modelling other control surfaces located closer to the root, such as flaperons.

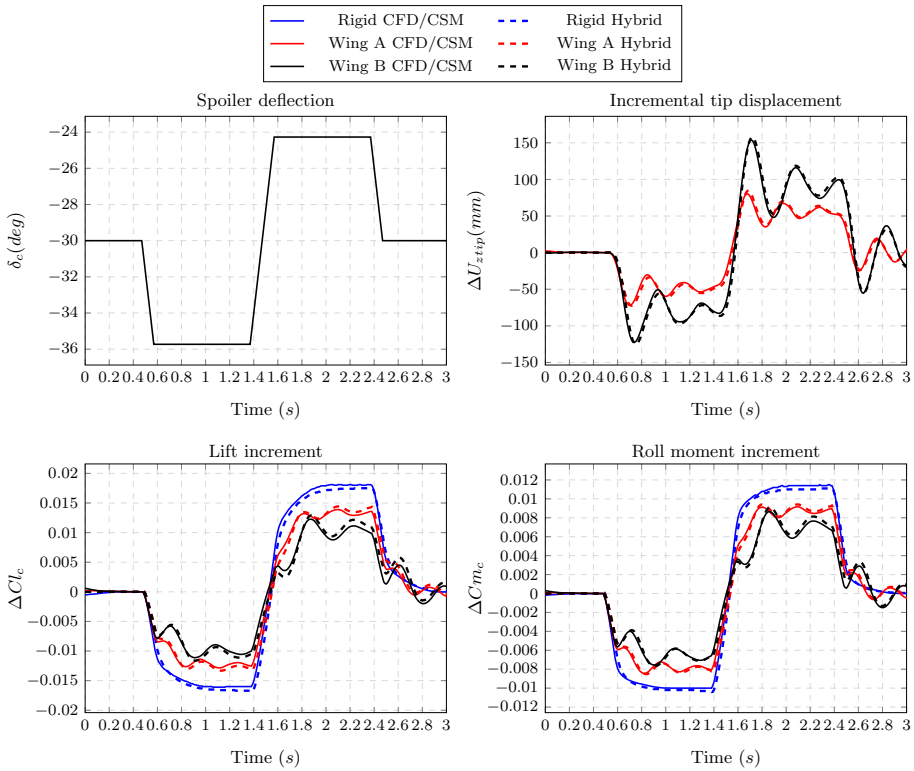

Figure 23: CFD/CSM compared against the hybrid model with dynamic spoiler deflections. The deflection range varies from -5.7 to +5.7 degrees around a baseline position of 30 degrees.

6. Conclusions

In this paper, we have introduced a data-driven method to capture the unsteady non-linear incremental loads from arbitrary aileron and spoiler motion. For a given device, Mach number and dynamic pressure, we perform several steady-state CFD analyses with a range of rotation angles to fill-up look-tables capturing the static non-linear aerodynamic behaviour of the control surface. We then perform a single transient CFD analysis with small control deflections to capture the unsteady effects. This approach makes it possible to use standard dynamic smoothing deformation techniques without risk of stretching the mesh excessively. Before identifying the transfer functions, we remove the steady aerodynamic component of the transient CFD response from the training data using the look-up tables. We do this to perform the transfer functions identification on the unsteady linear aerodynamic component of the control response. Finally, we sum up the unsteady linear and steady non-linear aerodynamic contributions to restitute the complete control loads. We first demonstrated the accuracy of this method on a 2D transonic rigid airfoil geometry equipped with an aileron. We compared the results given by our model against transient CFD-RANS analyses for a wide range of deflection rates and amplitudes. Results showed that for most of the realistic rate/amplitude combinations, our method was effective to replicate CFD results, predicting the lift increment within a 5% error margin. Our model also showed a better prediction than linearised or quasi-steady approximations.

Then we tested our methodology on a realistic 3D transonic rigid wing equipped with an aileron and a spoiler. The spoiler is a control surface which is difficult to approximate using potential flow theory because it inherently creates flow separation. Its modelling is restricted to empirical models, or CFD and higher-order methods which are computationally expensive. We approached this problem by discretizing our wing in spanwise strips, on which incremental loads from CFD simulations are integrated to create local ROMs capturing the load increments along the span from the movable deflection. As for the 2D example, we only

needed for the ROM identification one transient simulation with small deflection amplitudes and nine static CFD analyses. Using the resulting ROM, we were able to replicate the incremental loads calculated with transient CFD for any arbitrary spoiler motion. We also obtained good results with the aileron, for which the ROM yielded a good agreement against the reference CFD simulations.
Finally, we developed and compared an approach where we combined our aerodynamic ROM with a linear aeroelastic solver, the SOL146 from MSC NASTRAN. Here, the non-linear unsteady rigid incremental loads from control deflections are super-imposed on the aeroelastic solution. With this method, we can capture the loss of control effectiveness due to both non-linear aerodynamic and linear aeroelasticity. We benchmarked our approach against conventional time marching coupled CFD/CSM in the transonic regime. The results with the aileron showed a good agreement with our hybrid model when the wing is moderately flexible (wing A). For the more flexible cases (wing B), the difference is higher but remains within 13%. The results with the spoiler are also promising, with the error on the tip displacement, lift and moment increment coefficients below 6%.
The ROM and the hybrid approach presented could be of great benefice during the aircraft preliminary sizing, which today mostly relies on linear aeroelastic models or databases of fixed loads identified from higher-fidelity methods. One advantage of our process is that it is entirely non-intrusive and is solver agnostic. The ROM can be identified from higher-fidelity analyses or wind tunnel data and requires relatively few runs to be built from. At the same time, a wide range of aeroelastic solvers can be used for flexible cases. The follow-up work could include the investigation of simultaneous control surfaces deflections, as well as a broader exploration of the flight envelope of a typical transport aircraft.

Acknowledgments

The authors would like to thank Daniel Piñeiro Rielo for the dynamic CFD/CSM framework he developed during his internship at the Delft University of Technology and used here for comparison.

References

[1] Ansys fluent 12.0 theory guide - 3.3.1 dynamic mesh update methods. https://www.afs.enea.it/project/neptunius/docs/fluent/html/th/node40.htm.

[2] Ansys fluent 12.0 theory guide - 4.5.2 shear-stress transport (sst) - model. https://www.afs.enea.it/project/neptunius/docs/fluent/html/th/node67.htm.

[3] Simulink - Simulation and Model-Based Design - MATLAB & Simulink. https://nl.mathworks.com/products/simulink.html.

[4] Transfer function estimation - matlab tfest. https://nl.mathworks.com/help/ident/ref/tfest.html.

[5] P. Bekemeyer, R. Thormann, and S. Timme. Investigation into gust load alleviation using computational fluid dynamics. In *18th International Forum on Aeroelasticity and Structural Dynamics*, June 2019. https://livrepository.liverpool.ac.uk/3046290/1/IFASD-2019-068.pdf.

[6] X. Bertrand. *Modélisation aérodynamique des surfaces de contrôle de la voilure d'un avion de transport*. Phd thesis, Toulouse, ISAE, January 2008. https://depozit.isae.fr/theses/2008/2008_Bertrand_Xavier.pdf.

[7] T. R. Brooks, G. K. W. Kenway, and J. R. R. A. Martins. Benchmark aerostructural models for the study of transonic aircraft wings. *AIAA Journal*, 56(7):2840–2855, June 2018. https://arc.aiaa.org/doi/10.2514/1.J056603.

[8] T. S. Chyczewski, M. Dubiel, D. R. McDaniel, M. Foster, M. A. Niestroy, S. M. Klausmeyer, W. A. Silva, D. D. Vicroy, C. Hummer, W. Thomas, and B. E. Green. A position on current stability and control prediction capabilities and a path forward. In *AIAA Aviation 2020 Forum*. American Institute of Aeronautics and Astronautics, June 2020. https://arc.aiaa.org/doi/pdf/10.2514/6.2020-2678.

[9] J. K. S. Dillinger, M. M. Abdalla, Y. M. Meddaikar, and T. Klimmek. Static aeroelastic stiffness optimization of a forward swept composite wing with cfd-corrected aero loads. *CEAS Aeronautical Journal*, 10, May 2019. https://link.springer.com/article/10.1007/s13272-019-00397-y.

[10] G. Fillola. *Étude expérimentale et simulations numériques d'écoulements autour des surfaces mobiles de voilure*. Phd thesis, Toulouse, ENSAE, January 2006. https://depozit.isae.fr/theses/2006/2006_Fillola_Guillaume.pdf.

[11] F. Gand. Zonal detached eddy simulation of a civil aircraft with a deflected spoiler. *AIAA Journal*, 51(3):697–706, 2013. https://arc.aiaa.org/doi/10.2514/1.J052106.

[12] M. Ghoreyshi and R. M. Cummings. Unsteady aerodynamic modeling of aircraft control surfaces by indicial response methods. *AIAA Journal*, 52(12):2683–2700, December 2014. https://arc.aiaa.org/doi/10.2514/1.J052946.

[13] P. Goggin. A general gust and maneuver load analysis method to account for the effects of active control saturation and nonlinear aerodynamics. In *Dynamics Specialists Conference*. American Institute of Aeronautics and Astronautics, April 1992. https://arc.aiaa.org/doi/abs/10.2514/6.1992-2126.

[14] R. Halder, M. Damodaran, and B. C. Khoo. Signal interpolation augmented linear nonintrusive reduced-order model for aeroelastic applications. *AIAA Journal*, 58(1):426–444, 2020. https://doi.org/10.2514/1.J058529.

[15] B. R. Hiller, N. T. Frink, W. A. Silva, and D. N. Mavris. Aeroelastic indicial response reduced-order modeling for flexible flight vehicles. *Journal of Aircraft*, pages 1–22, January 2020. https://doi.org/10.2514/1.C035646.

[16] R. Huang, H. Liu, Z. Yang, Y. Zhao, and H. Hu. Nonlinear reduced-order models for transonic aeroelastic and aeroservoelastic problems. *AIAA Journal*, 56(9):3718–3731, September 2018. https://arc.aiaa.org/doi/10.2514/1.J056760.

[17] A. Huebner and L. Reimer. Gust encounter simulations of a generic transport aircraft and analysis of load alleviation potentials by control surface deflections using a rans-cfd-based multidisciplinary simulation environment. In *AIAA Aviation 2019 Forum*. American Institute of Aeronautics and Astronautics, 2019. https://arc.aiaa.org/doi/pdf/10.2514/6.2019-3198.

[18] F. Huvelin, P. Girodroux Lavigne, and C. Blondeau. High fidelity numerical simulations for gust response analysis. In *15th International Forum on Aeroelasticity and Structural Dynamics*, June 2013.

[19] E. H. Johnson and W. P. Rodden. Msc nastran version 68 aeroelastic analysis user's guide. *MSC Software Aeroelastic Guide*, 1994.

[20] T. Klimmek. Development of a structural model of the crm configuration for aeroelastic and loads analysis. *Journal of Aeroelasticity and Structural Dynamics*, 3(2):31–49, May 2014. https://www.asdjournal.org/index.php/ASD/article/viewFile/27/Klimmek_ASDJ2014.pdf.

[21] P. M. G. J. Lancelot and R. De Breuker. Passively actuated spoiler for gust load alleviation. In *27th International Conference on Adaptive Structures and Technologies*, October 2016. http://resolver.tudelft.nl/uuid:29f86d2a-7cd1-4159-96a2-c880a5b9c53d.

[22] P. M. G. J. Lancelot and R. De Breuker. Transonic flight and movable load modelling for wing-box preliminary sizing. In *18th International Forum on Aeroelasticity and Structural Dynamics*, June 2019. http://resolver.tudelft.nl/uuid:305d8d69-c069-480d-a674-f650316d8935.

[23] L. Liu, A. K. Padthe, P. P. Friedmann, E. Quon, and M. J. Smith. Unsteady aerodynamics of an airfoil/flap combination on a helicopter rotor using computational fluid dynamics and approximate methods. *Journal of the American Helicopter Society*, 56:32003, July 2011. https://www.ingentaconnect.com/content/ahs/jahs/2011/00000056/00000003/art00004.

[24] E. Livne. Aircraft active flutter suppression: State of the art and technology maturation needs. *Journal of Aircraft*, 55(1):410–450, December 2018. https://arc.aiaa.org/doi/10.2514/1.C034442.

[25] MSC Software Corporation. Msc nastran quick reference guide. 2009. https://simcompanion.mscsoftware.com/infocenter/index?page=content&id=DOC9106.

[26] D. Piñeiro Rielo. *Development of a Fluid-Structure Interaction simulation algorithm for the analysis of the static and dynamic*. Master's thesis, Universidade de Vigo (Spain) - Delft University of Technology (The Netherlands), November 2019.

[27] A. Prachař, P. Hospodář, and P. Vrchota. Gust alleviation of aeroelastic aircraft using cfd simulation. *Transportation Research Procedia*, 29:366–375, 2018. http://www.sciencedirect.com/science/article/pii/S2352146518300371.

[28] M. Pusch, A. Knoblach, and T. Kier. Integrated optimization of control surface layout for gust load alleviation. *CEAS Aeronautical Journal*, 1:3, February 2019. https://link.springer.com/article/10.1007/s13272-019-00367-4.

[29] H. D. Ramsey and J. G. Lewolt. Design maneuver loads for an airplane with an active control system. In *20th Structures, Structural Dynamics, and Materials Conference*. American Institute of Aeronautics and Astronautics, April 1979. https://arc.aiaa.org/doi/10.2514/6.1979-738.

[30] D. Raveh. Cfd-based gust response analysis of free elastic aircraft. *Journal of Aeroelasticity and Structural Dynamics*, 2(1), May 2010. https://www.asdjournal.org/index.php/ASD/article/view/3.

[31] L. Reimer, R. Heinrich, and M. Ritter. Towards higher-precision maneuver and gust loads computations of aircraft: Status of related features in the cfd-based multidisciplinary simulation environment flowsimulator. In *New Results in Numerical and Experimental Fluid Mechanics XII*, pages 597–607. Springer International Publishing, September 2019. https://link.springer.com/chapter/10.1007/978-3-030-25253-3_57.

[32] C. Riso, D. Sanghi, and C. E. S. Cesnik. Parametric roll maneuverability analysis of a high-aspect-ratio-wing civil transport aircraft. In *AIAA Scitech Forum*. American Institute of Aeronautics and Astronautics, January 2020. https://arc.aiaa.org/doi/10.2514/6.2020-1191.

[33] M. Ritter and M. S. Roeser. Cfd-based multi-axis maneuver simulation for system identification of flexible transport aircraft. In *AIAA Scitech Forum*, January 2020. https://arc.aiaa.org/doi/abs/10.2514/6.2020-2125.

[34] R. B. Seidler, S. Marten, M. Widhalm, and J. Wild. Efficient prediction of aerodynamic control surface responses using the linear frequency domain. *AIAA Journal*, 58(5):1964–1975, February 2020. https://arc.aiaa.org/doi/10.2514/1.J058840.

[35] O. Sensburg, J. Becker, H. Lusebrink, and F. Weiss. Gust load alleviation on airbus a300. In *13th Congress of International Council of the Aeronautical Sciences (ICAS)*, September 1982. http://www.icas.org/ICAS_ARCHIVE/ICAS1982/ICAS-82-2.1.1.pdf.

[36] B. Stickan, R. Thormann, and H. Bleecke. Control surface modelling of unsteady large amplitude motion via chimera cfd technique. In *International Forum on Aeroelasticity and Structural Dynamics*, June 2019. https://www.asdjournal.org/public/Proceedings/IFASD_2019/IFASD-2019-015.pdf.

[37] F. G. Di Vincenzo and A. Castrichini. Msc nastran hybrid static aeroelasticity integrated, accurate static aeroelastic analysis with cfd data. Technical report, 2013.

[38] J. M. Waite, B. K. Stanford, W. A. Silva, and R. E. Bartels. Reduced order modeling for transonic aeroservoelastic control law development. In *AIAA Scitech Forum*, January 2019. https://arc.aiaa.org/doi/pdf/10.2514/6.2019-1022.

[39] L. Wiart and G. Carrier. Accounting for wing flexibility in the aerodynamic calculation of transport aircraft using equivalent beam model. In *13th AIAA/ISSMO Multidisciplinary Analysis and Optimization Conference*, June 2012. https://arc.aiaa.org/doi/10.2514/6.2010-9135.

[40] W. Wilkinson, T. Lines, and N. Yu. Navier-stokes calculations for massively separated flows. In *14th Applied Aerodynamics Conference*, June 1996. https://arc.aiaa.org/doi/abs/10.2514/6.1996-2383.